Multiple superconducting transitions in the $Sr_3Ru_2O_7$ region of $Sr_3Ru_2O_7$-Sr_2RuO_4 eutectic crystals

S. Kittaka,[1] S. Fusanobori,[1] S. Yonezawa,[1] H. Yaguchi,[1] Y. Maeno,[1,2] R. Fittipaldi,[1,2,3] and A. Vecchione[1,2,3]
[1]*Department of Physics, Kyoto University, Kyoto 606-8502, Japan*
[2]*International Innovation Center, Kyoto University, Kyoto 606-8501, Japan*
[3]*CNR-INFM Regional Laboratory "SuperMat" and Department of Physics, University of Salerno, I-84081 Baronissi (Sa), Italy*
(Received 27 June 2006; revised manuscript received 14 August 2007; published 13 June 2008)

We report the superconducting properties of $Sr_3Ru_2O_7$-Sr_2RuO_4 eutectic crystals, which consist of the spin-triplet superconductor Sr_2RuO_4 with a monolayer stacking of RuO_2 planes and the metamagnetic normal metal $Sr_3Ru_2O_7$ with a bilayer stacking. Although $Sr_3Ru_2O_7$ so far has not been reported to exhibit superconductivity, our ac susceptibility measurements revealed multiple superconducting transitions that occur in the $Sr_3Ru_2O_7$ region of the eutectic crystals. The diamagnetic shielding essentially reached the full fraction at low ac fields parallel to the *c* axis. However, both the shielding fraction and the onset temperature are easily suppressed by ac fields larger than 0.1 mT rms and no anomaly was observed in the specific heat. Moreover, the critical field curves of these transitions have a positive curvature near zero fields, which is different from the upper critical field curve of the bulk Sr_2RuO_4. These facts suggest that the superconductivity observed in the $Sr_3Ru_2O_7$ region is not a bulk property. To explain these experimental results, we propose the scenario that stacking RuO_2 planes, which are the building blocks of superconducting Sr_2RuO_4, are contained in the $Sr_3Ru_2O_7$ region as stacking faults.

DOI: 10.1103/PhysRevB.77.214511 PACS number(s): 74.70.Pq, 74.50.+r, 74.81.Bd

I. INTRODUCTION

The layered perovskite superconductor Sr_2RuO_4 (T_c = 1.5 K), which is isostructural to the high-T_c cuprate $La_{2-x}Sr_xCuO_4$, is now believed to be a spin-triplet superconductor with broken time-reversal symmetry based on various experimental results.[1–5] After the discovery of superconductivity in Sr_2RuO_4, two types of eutectic solidification systems containing Sr_2RuO_4 have been grown: Sr_2RuO_4-Ru (Ref. 6) and $Sr_3Ru_2O_7$-Sr_2RuO_4.[7] These eutectic systems are also interesting because they exhibit unusual superconducting features.

The Sr_2RuO_4-Ru eutectic system,[6] in which lamellae of Ru metal are embedded in Sr_2RuO_4, exhibits a large enhancement in T_c. From ac susceptibility measurements[6] it was revealed that a broad diamagnetic transition occurs with an onset temperature as high as 3 K, which is twice higher than those of best-quality Sr_2RuO_4 single crystals. Therefore, this eutectic is referred to as the 3–K phase. However, specific-heat measurements[8] revealed that the volume fraction of the superconductivity associated with the 3–K phase is very small. Measurements of the tunneling conductance between Sr_2RuO_4 and a single Ru lamella[9,10] support that the superconductivity with an enhanced T_c occurs in the boundaries between the Sr_2RuO_4 and the embedded Ru lamella.

We have recently succeeded in growing another Sr_2RuO_4-based eutectic system:[7] $Sr_3Ru_2O_7$-Sr_2RuO_4. This eutectic system consists of the spin-triplet superconductor Sr_2RuO_4 with a monolayer stacking of RuO_2 planes and the metamagnetic normal metal[11,12] $Sr_3Ru_2O_7$, which consists of a bilayer stacking. X-ray diffraction analyses of the $Sr_3Ru_2O_7$-Sr_2RuO_4 eutectic crystals indicated that the directions not only of the *c* axis but also of the in-plane axes of Sr_2RuO_4 and $Sr_3Ru_2O_7$ are common in the eutectic crystals.[7] The superconductivity observed in this eutectic crystal also exhibits interesting features. From ac susceptibility measurements[7] of a eutectic sample containing a number of Sr_2RuO_4 and $Sr_3Ru_2O_7$ domains, it was revealed that a superconducting transition occurs at 1.43 K and the diamagnetic shielding fraction keeps increasing upon cooling well below T_c. It was speculated that this additional diamagnetic signal was due to a proximity effect into $Sr_3Ru_2O_7$ from superconducting Sr_2RuO_4.[7]

Subsequently, a finite superconducting critical current in a $Sr_3Ru_2O_7$-Sr_2RuO_4 eutectic system containing many Sr_2RuO_4 and $Sr_3Ru_2O_7$ domains was observed by Hooper *et al.*[13] Their finding appears to indicate that $Sr_3Ru_2O_7$ domains are also superconducting. They suggested the possibility of a proximity effect in the $Sr_3Ru_2O_7$ regions with an unusually long coherence length. In fact, the coherence length ξ_N in $Sr_3Ru_2O_7$ due to a proximity effect must be as long as the size of $Sr_3Ru_2O_7$ domains, which is a few hundred micrometers, if supercurrent flows across the $Sr_3Ru_2O_7$ regions. However, the conventional coherence length of a proximity effect in a clean limit approximation yields $\xi_N \sim 0.17$ μm at 0.3 K. This value of the conventional coherence length is too short to account for the superconductivity in $Sr_3Ru_2O_7$.

In the present study, we investigated the temperature dependence of ac susceptibility at various ac and dc fields by using $Sr_3Ru_2O_7$-Sr_2RuO_4 eutectic samples consisting of one Sr_2RuO_4 region and one $Sr_3Ru_2O_7$ region with a single boundary between them [e.g., see the insets of Figs. 1(a) and 2]. Measurements of these samples revealed that the apparent superconducting volume fraction of the $Sr_3Ru_2O_7$-Sr_2RuO_4 eutectic sample was as large as 100%. In order to test the proximity scenario, we performed similar measurements with the $Sr_3Ru_2O_7$ region cut from a eutectic crystal and, surprisingly, we also observed superconductivity with a very large apparent volume fraction. These results indicate that the superconductivity with a large apparent volume fraction

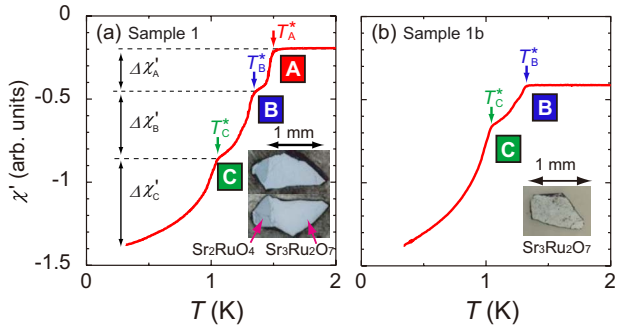

FIG. 1. (Color online) Temperature dependence of the real part of the ac susceptibility at $\mu_0 H_{ac}=0.58$ μT rms and $\mu_0 H_{dc}=0$ T: (a) for sample 1 ($Sr_3Ru_2O_7$-Sr_2RuO_4 eutectic); (b) for sample 1b (i.e., the $Sr_3Ru_2O_7$ region cut from sample 1). The insets are PLOM images of the samples.

occurs in the $Sr_3Ru_2O_7$ region and that its origin cannot be attributed to the proximity effect from the bulk Sr_2RuO_4 region. In addition, we did not observe any anomaly in the specific heat of the $Sr_3Ru_2O_7$ region. Also, we calculated the temperature dependence of the ac susceptibility based on a multiple superconductor model (scenario II in Sec. IV) and obtained calculated results which match well with our experimental results.

II. EXPERIMENT

In this paper, we mainly present data that were obtained by using a sample cut from a $Sr_3Ru_2O_7$-Sr_2RuO_4 eutectic crystal (batch Cfv07 in Ref. 7), which was grown with a floating-zone furnace. We carefully chose a $Sr_3Ru_2O_7$-Sr_2RuO_4 eutectic part, which has only one boundary between Sr_2RuO_4 and $Sr_3Ru_2O_7$ (hereafter referred to as sample 1). The size of sample 1 was approximately $1.5 \times 0.7 \times 0.3$ mm^3. The inset of Fig. 1(a) shows polarized light optical microscopy (PLOM) images of polished *ab* planes of sample 1. The darker area of the sample is the Sr_2RuO_4 region and the brighter area is the $Sr_3Ru_2O_7$ region, which was confirmed by a high resolution x-ray diffractometer[7] and energy dispersive x-ray (EDX) analysis. Sample 1 certainly consists of one bulk Sr_2RuO_4 region and one bulk $Sr_3Ru_2O_7$ region because the top and bottom surfaces have the same eutectic pattern. In order to check the reproducibility of experimental results, we performed measurements with more than ten eutectic samples [one of them is sample 2 from batch Cfv07, which is shown in the inset of Fig. 2(c)]. Eutectic samples from different batches qualitatively exhibit the same behavior, too.

We measured the ac magnetic susceptibility, $\chi_{ac}=\chi'+i\chi''$, by a mutual-inductance technique by using a lock-in amplifier at various frequencies ranging from 19 to 3011 Hz. The data shown below were all taken at 3011 Hz because the frequency dependence of χ_{ac} was found to be insignificant. The ac susceptibility was measured down to 0.3 K by using a ^{3}He cryostat with a 2 T magnet (Oxford Instruments) and down to 20 mK by using a ^{3}He-^{4}He dilution refrigerator (Cryoconcept) with an 11 T magnet (Oxford Instruments). The ac field H_{ac} was applied parallel to the *c* axis or the *ab* plane with a small coil (40 μT/mA), and the dc field H_{dc} was applied parallel to H_{ac}. In this paper, we mainly report results under magnetic fields parallel to the *c* axis. When we measured χ_{ac} in zero dc field, we used a high-permeability-metal shield to exclude the geomagnetic field of about 50 μT. The resultant residual field in this shield was estimated to be lower than 0.1 μT.

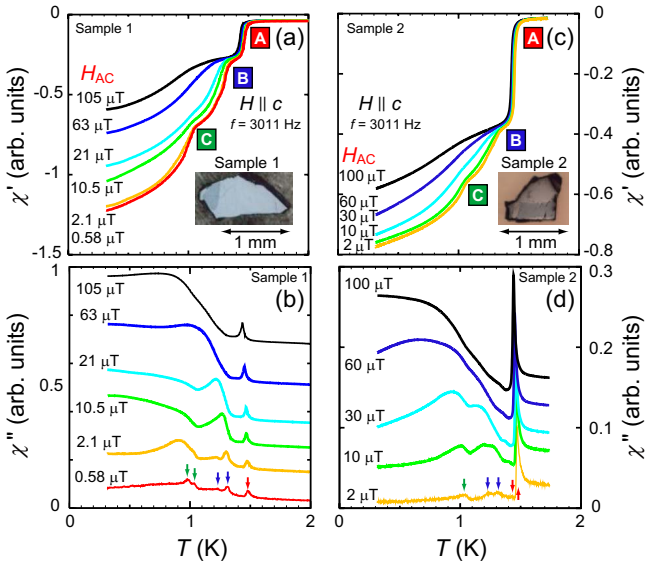

FIG. 2. (Color online) Temperature dependence of the ac susceptibility of $Sr_3Ru_2O_7$-Sr_2RuO_4 eutectic crystals in various ac magnetic fields ($H_{ac} \| c$, $\mu_0 H_{dc}=0$ T). (a) and (b) represent the real and imaginary parts of χ_{ac} of sample 1, respectively. (c) and (d) represent those of sample 2. The insets are PLOM images of the samples. The numbers labeling the curves give the applied ac field amplitude $\mu_0 H_{ac}$ in μT rms.

We also measured the specific heat c_p of the eutectic samples by a thermal relaxation method with a commercial calorimeter (Quantum Design, PPMS) from 30 to 0.8 K. The $Sr_3Ru_2O_7$-Sr_2RuO_4 eutectic crystals were characterized by x-ray diffraction (XRD) with Cu Kα_1 radiation and EDX analysis.

III. RESULTS

A. ac susceptibility measurement

Figure 1(a) shows the temperature dependence of the ac susceptibility of sample 1 ($Sr_3Ru_2O_7$-Sr_2RuO_4 eutectic crystal) under $\mu_0 H_{ac}=0.58$ μT rms and $\mu_0 H_{dc}=0$ T with a high-permeability-metal shield. In this measurement, we observed three steep changes of the diamagnetic signal in χ', which we will hereafter call transitions A, B, and C. The transition temperatures, which are defined as the onset temperatures of the transitions in χ', were 1.48, 1.33, and 1.04 K and are hereafter labeled T_A^*, T_B^*, and T_C^*, respectively. Although more peaks were observed in χ'' [marked with the arrows in Fig. 2(b)], we mainly focus on transitions A, B, and C. It was difficult to accurately evaluate the shielding fraction because of the large demagnetization factor of the sample. By comparing the diamagnetic signal $\Delta\chi'$ of sample 1, which is equal to $\Delta\chi'_A+\Delta\chi'_B+\Delta\chi'_C$, as shown in Fig. 1(a), with that of

a pure Sr_2RuO_4 crystal with dimensions similar to those of sample 1, we evaluated the apparent shielding fraction of sample 1 to be approximately 100% at 0.3 K. This large shielding fraction implies that the superconducting screening current flows not only in the Sr_2RuO_4 part of the sample but also in most of the $Sr_3Ru_2O_7$ region.

In order to clarify whether or not this superconductivity is attributed to an unusual proximity effect from the boundary of the bulk Sr_2RuO_4, we completely removed the bulk Sr_2RuO_4 part from sample 1, which is hereafter labeled sample 1b. The dimension of sample 1b is approximately $1.0\times0.6\times0.15$ mm^3. The inset of Fig. 1(b) is a PLOM image of sample 1b. As presented in Fig. 1(b), two of the superconducting transitions were still observed in sample 1b. The transition temperatures were 1.32 and 1.04 K, corresponding well to T_B^* and T_C^* in sample 1. The absence of transition A in sample 1b proves that transition A originates from the bulk Sr_2RuO_4 part of sample 1 and that transitions B and C occur in the $Sr_3Ru_2O_7$ region. The apparent shielding fraction of sample 1b was estimated to be 90% for $H\|c$ from the diamagnetic signal, $\Delta\chi'(=\Delta\chi'_B+\Delta\chi'_C)$. In contrast, it was estimated to be less than 1% for $H\|ab$ (not shown). These facts indicate that the superconducting screening current mainly flows within the *ab* planes. From these measurements, we conclude that the $Sr_3Ru_2O_7$ region in the eutectic crystal has multiple superconducting transitions, although pure $Sr_3Ru_2O_7$ has not been reported to become superconducting down to 20 mK.[11] Moreover, it is clear that the origin of the superconductivity observed in the $Sr_3Ru_2O_7$ region is not a proximity effect from the bulk Sr_2RuO_4 part of the eutectic crystals across the boundary.

We revealed that *both* T^* and $\Delta\chi'$ of transitions B and C are extremely sensitive to the amplitude of H_{ac} when H_{ac} is parallel to the *c* axis. Figures 2(a) and 2(b) represent χ' and χ'' of sample 1 in different ac magnetic fields. We normalized the obtained signals with respect to the strength of H_{ac}. As shown in Fig. 2(a), T_A^* and $\Delta\chi'_A$ hardly depend on H_{ac} up to 100 μT rms. In contrast, $\Delta\chi'_B$ and $\Delta\chi'_C$ are severely suppressed by H_{ac} of less than 100 μT rms. In addition, T_B^* and T_C^* are easily shifted toward lower temperatures with increasing the ac field amplitude. As represented in Figs. 2(c) and 2(d), we reproducibly observed these features in other samples. However, when H_{ac} is applied parallel to the *ab* plane, T^* and $\Delta\chi'$ of transitions B and C are not sensitive to H_{ac} of less than 100 μT rms.

In order to obtain more information on transitions B and C, we measured the dc field dependence of χ_{ac} for sample 1b. Figure 3 shows the temperature dependence of χ' and χ'' at various dc fields and Fig. 4 presents the dc field dependence of χ' at several temperatures for sample 1b. In these measurements, we fixed the amplitude of H_{ac} to 1 μT rms, and both H_{ac} and H_{dc} were applied parallel to the *c* axis. These measurements revealed that T_B^* and T_C^* are *not* severely suppressed, but $\Delta\chi'_B$ and $\Delta\chi'_C$ are easily suppressed by H_{dc}.

We obtained the *H-T* phase diagram for $H\|c$, which is plotted in Fig. 5. Here, the critical fields of transitions B and C are labeled H_B^* and H_C^*, respectively, which are defined as the onset of χ'. For comparison, we included the upper critical field H_{c2} of bulk Sr_2RuO_4 determined by specific-heat

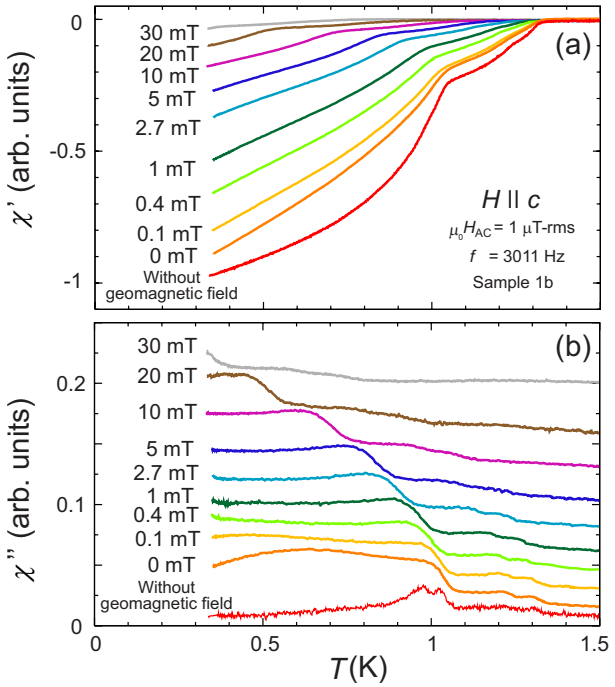

FIG. 3. (Color online) Temperature dependence of the (a) real and (b) imaginary parts of χ_{ac} of sample 1b in different dc fields.

measurements[14] and those determined by ac susceptibility measurements[15] in Fig. 5. The extrapolation of $\mu_0H_B^*$ to $T=0$ yields 75 mT, which is nearly equal to $\mu_0H_{c2}(T=0)$ of bulk Sr_2RuO_4.

However, the temperature dependences of H_B^* and of H_C^* are qualitatively different from that of $H_{c2}(T)$ of bulk Sr_2RuO_4. Fitting the function $H_{c2}(T)=\alpha(1-T/T_c)^n$ to the H_{c2} data from specific-heat measurements of bulk Sr_2RuO_4 yields $n=1.0$ for $H\|c$ near $H_{dc}=0$, where α and n are adjustable parameters. In contrast, both H_B^* and H_C^* exhibit temperature dependences with positive curvatures ($n=1.6$ for H_B^*, $n=1.5$ for H_C^*) near $H_{dc}=0$ and then approximately lin-

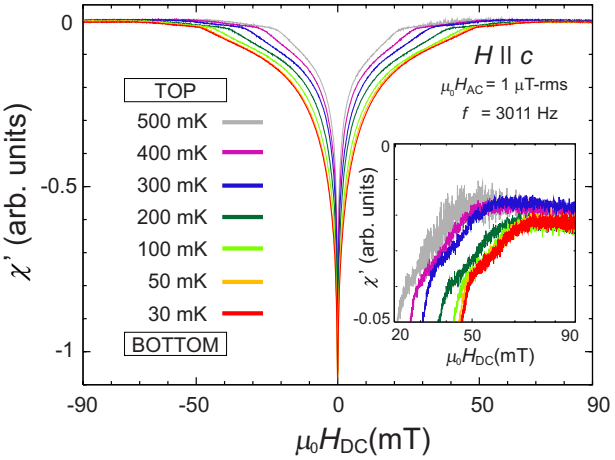

FIG. 4. (Color online) The dc field dependence of the real part of χ_{ac} of sample 1b. The inset gives an enlarged view near onset. In order to take the residual fields into account in our equipment, which are estimated to be approximately 1 mT, we determined zero field as a field at which χ' becomes minimum.

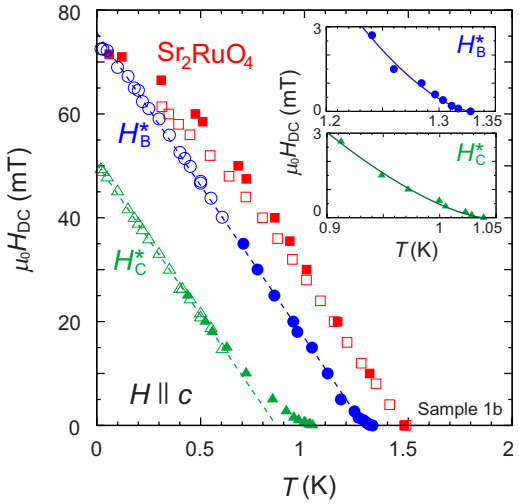

FIG. 5. (Color online) *H-T* phase diagram of sample 1b for $H_{ac} \| H_{dc} \| c$ determined from the ac susceptibility measurements. The circles and triangles represent the critical fields of transitions B and C, respectively. The open symbols are obtained from the field sweep data and the closed symbols are from the temperature sweep data. H_{c2} of bulk Sr_2RuO_4 from specific-heat data (Ref. 14, closed squares) and from ac susceptibility measurements (Ref. 15, open squares) are also plotted. The insets show the low-field region below 3 mT. The solid lines represent fits of the data close to $T_0^* \equiv T^*(H_{dc}=0)$ by using the function $\alpha(1-T/T_0^*)^n$. The dashed lines present results of linear fittings to the data between 0 K and 0.7 T_0^*.

early increase with decreasing temperature. Such behavior suggests that transitions B and C are of a similar origin but different from the bulk superconducting transition.

We also constructed the *H-T* phase diagram for $H \| ab$, as shown in Fig. 6. In this measurement, both H_{ac} of 20 μT rms and H_{dc} were applied parallel to the *ab* plane. Both the temperature dependences of H_B^* and of H_C^* exhibit a positive curvature near $H_{dc}=0$, similar to those for $H \| c$. The critical field anisotropies $H_{\|ab}^*/H_{\|c}^*$ of transitions B and C are approximately 13 at 0.3 K, which is somewhat smaller than that observed for bulk Sr_2RuO_4 (Ref. 16: $H_{c2\|ab}/H_{c2\|c} \sim 20$).

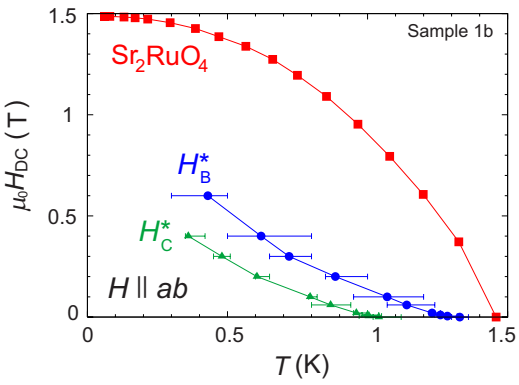

FIG. 6. (Color online) *H-T* phase diagram of sample 1b for $H_{ac} \| H_{dc} \| ab$. The circle and triangular symbols represent the critical fields of transitions B and C determined by the ac susceptibility measurements, respectively. The upper critical fields H_{c2} of bulk Sr_2RuO_4 are obtained from the ac susceptibility measurements (Ref. 15, squares). The solid lines are guides to the eye.

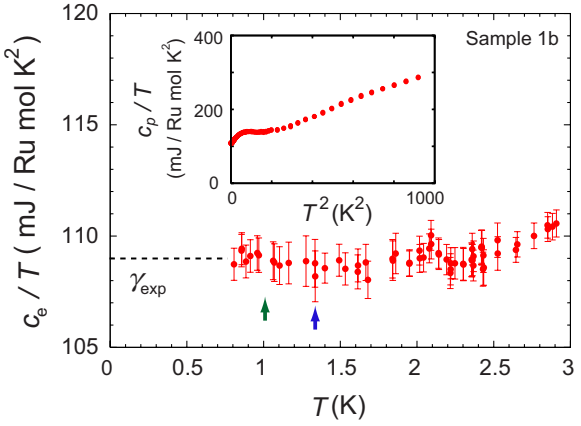

FIG. 7. (Color online) Temperature dependence of the electronic specific heat divided by temperature c_e/T of sample 1b. The inset represents c_p/T plotted against T^2. The arrows mark T_B^* and T_C^* of this sample at zero field.

B. Specific-heat measurement

We measured the specific heat of sample 1b (with a mass $m=0.472$ mg), which exhibits a nearly full diamagnetic shielding in our ac susceptibility measurements for $H \| c$. This specific-heat measurement was performed in zero field, but the geomagnetic field and the residual field of the magnet ($\lesssim 1$ mT) were not shielded. The main panel of Fig. 7 shows the electronic specific heat divided by temperature for sample 1b. There is no anomaly at T_B^* and T_C^*. Therefore, we conclude that the actual volume fraction of the superconductivity observed in the apparent $Sr_3Ru_2O_7$ region is very small.

In order to obtain the electronic specific-heat coefficient γ_{expt} of sample 1b and check the molar ratio x of Sr_2RuO_4 contained in sample 1b, we used an effective weight per Ru mole M_{eff}, which is defined as $M_{eff}(x)=xM_{214}+(1-x)M_{327}/2$, where M_{214} and M_{327} are the molar weights of a f.u. of Sr_2RuO_4 and $Sr_3Ru_2O_7$, respectively. We determined γ_{expt}, which is obtained from the relation $\gamma_{expt}(x)=(C_p/T)m/M_{eff}(x)$ (C_p is the heat capacity of the sample), self-consistently by adjusting x so that $\gamma_{expt}(x)$ becomes equal to $x\gamma_{214}+(1-x)\gamma_{327}$. Here, γ_{214} and γ_{327} represent the electronic specific-heat coefficient of bulk Sr_2RuO_4 [$\gamma_{214}=38$ mJ/Ru mol K^2 (Ref. 17)] and $Sr_3Ru_2O_7$ [$\gamma_{327}=110$ mJ/Ru mol K^2 (Ref. 18)], respectively. As a result, we obtained $\gamma_{expt} \sim 109$ mJ/Ru mol K^2 and $x=0.016 \pm 0.008$. In addition, the overall temperature dependence of the total specific heat c_p of sample 1b presented in the inset of Fig. 7 is consistent with previous reports[18] for pure $Sr_3Ru_2O_7$. These facts imply that the $Sr_3Ru_2O_7$ region of the eutectic crystals is almost the same as that of pure $Sr_3Ru_2O_7$.

C. Polarized light optical microscopy, energy dispersive x-ray, and x-ray diffraction analyses

In order to characterize the sample in more detail, we took PLOM images and performed elemental composition analysis with an EDX spectrometer and XRD analysis. From the

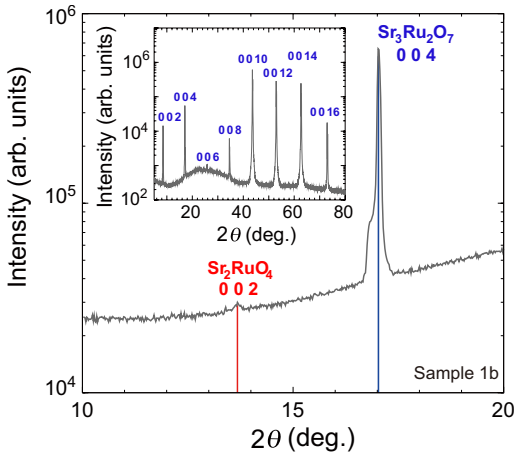

FIG. 8. (Color online) X-ray diffraction pattern for the *ab* plane of sample 1b. Note that the vertical axis is in a logarithmic scale.

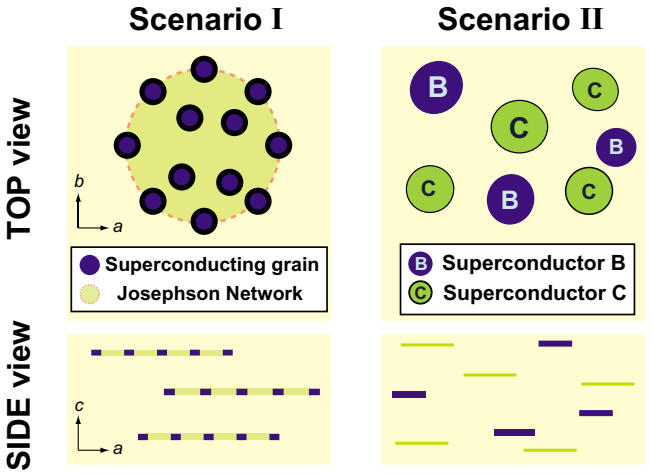

FIG. 9. (Color online) Scenarios for the superconductivity observed in the $Sr_3Ru_2O_7$ region of eutectic crystals are depicted. The superconducting regions are probably distributed along the *ab* planes because the shielding currents mainly flow within the *ab* planes. Such a layered arrangement is not taken into account in our simple model calculations.

PLOM images and elemental composition analysis, we did not find Sr_2RuO_4 and the whole sample seemed to consist of $Sr_3Ru_2O_7$. We note that we cannot rule out the presence of Sr_2RuO_4 parts with a size of less than about 1 μm, which is the experimental resolution limit of our instruments. In the XRD pattern for the *ab* plane of sample 1b, as shown in Fig. 8, a very weak $\langle 002 \rangle$ peak of Sr_2RuO_4 was detected in addition to strong $Sr_3Ru_2O_7$ peaks. The observed peak intensity suggests that less than a few percent Sr_2RuO_4 is contained at least in the surface region of sample 1b. This possible small content of Sr_2RuO_4 is consistent with the results of the specific-heat measurement.

IV. DISCUSSION

In order to discuss why superconductivity is observed in the $Sr_3Ru_2O_7$ region of eutectic crystals, we assumed two scenarios (scenarios I and II) and calculated $\chi_{ac}(T)$ for $H \| c$ by using simplified models.

A. Scenario I

First, we note that our results of $\chi_{ac}(T)$ is somewhat similar to those of granular superconductors, in which Josephson-type weak links are formed among superconducting grains. For example, polycrystals of $Tl_2Ba_2Ca_2Cu_3O_y$, which is prepared by a suitable sintering process, consist of agglomerates of grains whose typical size is approximately 5 μm.[19] These grains are randomly arranged and strongly connected by nonstoichiometric interfacial materials. When such polycrystals are cooled below T_c of the grains, the grains first become superconducting. Upon further cooling, Josephson-type weak links are formed among the grains. Therefore, shielding currents flow in intergrain paths and magnetic flux is excluded from the intergrain regions. As a result, two transitions, which are attributed to intragrain and intergrain superconductivities, are observed in $\chi_{ac}(T)$ and the transition temperature of the intergrain superconductivity is more sensitive to H_{ac} than to H_{dc}.[19] These features are observed in our results. Therefore, we first discuss the scenario wherein small superconducting Sr_2RuO_4 grains are embedded in the $Sr_3Ru_2O_7$ region of the eutectic crystals and superconducting networks are formed among them along *ab* planes (Fig. 9 left; scenario I).

Here, let us introduce a model developed by Müller[20] and Yang *et al.*[19] in order to calculate χ_{ac} of granular superconductors. Yang *et al.*[19] calculated $\chi_{ac}(T)$ of polycrystal $Tl_2Ba_2Ca_2Cu_3O_y$ by a method similar to Müller's[20] theoretical work, and their results reproduced well the experimental findings. Below, we calculate χ' and χ'' in the same way as Yang *et al.*[19] The sample shape is assumed to be a thin slab with thickness $2d$ in the x direction. The length in the y direction and height in the z direction of the sample are assumed to be infinity. The applied field $H_a(t) = \sqrt{2}H_{ac}\cos(\omega t) + H_{dc}$ is parallel to the slab's z direction. To avoid the complication of demagnetization factors, the grains are approximated as infinitely long superconducting cylinders aligned along the z direction. Instead, effects of finite demagnetization factors are embedded in other parameters, as we will explain below. The grain radius is assumed to be the same value R_g ($\ll 2d$), which represents the average grain radius in the experiments, for all the grains.

The real and imaginary parts of χ_{ac} are expressed as

$$\chi' = \frac{\omega}{\sqrt{2}\pi\mu_0 H_{ac}} \int_0^{2\pi/\omega} \langle B(t) \rangle \cos(\omega t) dt - 1, \tag{1}$$

$$\chi'' = \frac{\omega}{\sqrt{2}\pi\mu_0 H_{ac}} \int_0^{2\pi/\omega} \langle B(t) \rangle \sin(\omega t) dt. \tag{2}$$

Here, $\langle B(t) \rangle$ is the spatial average local flux density over the sample cross section and is given by $\langle B(t) \rangle = \langle B_J(t) \rangle_x + \langle \langle B_g(t) \rangle \rangle_{r,x}$. $\langle B_J(t) \rangle_x$ and $\langle \langle B_g(t) \rangle \rangle_{r,x}$ are the spatial average over the sample of the intergrain flux density $B_J(x,t)$ and that of the average intragrain flux density threading a cylindrical grain $\langle B_g(x,t) \rangle_r$, respectively. These notations are the same as those given by Müller.[20]

Let us now derive the inter- and intragrain magnetic field distributions by using the critical state equations[20] in order to obtain $\langle B_J(t)\rangle_x$ and $\langle\langle B_g(t)\rangle\rangle_{r,x}$. For the intergrain regions, the magnetic flux density B_J is larger than $\mu_0 H_J$ because the magnetic flux is compressed into the intergrain regions due to the diamagnetism of the superconducting grains. By embedding this effect into the effective permeability $\mu_{\rm eff}$, B_J can be expressed as $B_J=\mu_{\rm eff}\mu_0 H_J$. The effective permeability $\mu_{\rm eff}(T)$ is written as[21–23] $\mu_{\rm eff}(T)=f_n+f_s F[R_g/\lambda_g(T)]$, where $\lambda_g(T)$ denotes the London penetration depth of the superconducting grains, which depends on T as $\lambda_g(T)=\lambda_g(0)[1-(T/T_{cg})^4]^{-1/2}$. The factor f_s is the area fraction of the projection of grains onto a plane normal to the magnetic field, and f_n is that of the intergrain regions ($f_n=1-f_s$). The flux penetration within the surface penetration depth of the grains in the Meissner state is taken into account via $F(x)$, which is written as $F(x)=2I_1(x)/[xI_0(x)]$; I_0 and I_1 are the modified Bessel functions of the first kind. The intergrain magnetic field distribution H_J is given by the solution of the critical state equations:[20]

$$J_{cJ}(x,t)=\frac{\alpha_J(T)}{\mu_{\rm eff}(T)\mu_0}\frac{1}{|H_J(x,t)|+H_{0J}}, \tag{3}$$

$$\frac{dH_J(x,t)}{dx}=\pm J_{cJ}(x,t), \tag{4}$$

where we assume that the pinning force α_J of a vortex is equal to the Lorentz force.[24] The pinning force α_J is assumed to depend on T as[19] $\alpha_J(T)/\mu_{\rm eff}(T)=\alpha_J(0)(1-T/T_{cJ})^2/\mu_{\rm eff}(0)$, and H_{0J} is a positive parameter. The $\pm$ signs account for the outward or inward motion of vortices with decreasing or increasing applied magnetic field, respectively.

While we also assume the critical state for the intragrain regions, here, we used $B_g(r,x,t)$, which is equal to $\mu_0[H_g^{\rm ext}(x,t)+M_g(r,x,t)]$, where $H_g^{\rm ext}$ is the magnetic field at the boundary of a grain and M_g is the local magnetization in the grain because M_g is finite in the grains. $B_g(r,x,t)$, which is equivalent to $\mu_0 H_g(r,x,t)$ in Müller's[20] work, is obtained by the solution of the following equations:

$$J_{cg}(r,x,t)=\frac{\alpha_g(T)}{|B_g(r,x,t)|+B_{0g}}, \tag{5}$$

$$\frac{1}{\mu_0}\frac{dB_g(r,x,t)}{dr}=\pm J_{cg}(r,x,t). \tag{6}$$

In this case, the pinning force α_g is assumed[20] to be $\alpha_g(T)=\alpha_g(0)[1-(T/T_{cg})^2]^2$. B_{0g} is a positive parameter. We note that the effects of demagnetization factors are embedded in $\alpha_g(0)$ and B_{0g}. For example, if the demagnetization factor is large, $\alpha_g(0)/B_{0g}$ would become large. This calculation process is shown in Ref. 20. By solving Eqs. (3)–(6), we obtain $H_J(x,t)$ and $B_g(r,x,t)$, from which we can calculate $\langle B_J(t)\rangle_x$ and $\langle\langle B_g(t)\rangle\rangle_{r,x}$. By putting these quantities into Eqs. (1) and (2), we obtain χ' and χ''. Hereafter, we call this model the Müller–Yang model.

In this calculation, we fixed T_{cg}, T_{cJ}, and d to the values obtained from the present measurements, i.e., $T_{cg}=1.34$ K, $T_{cJ}=1.10$ K, and $d=1$ mm, and $\lambda_g(0)$ to the known value for the bulk Sr_2RuO_4. We varied the other parameters so that the calculated results best agree with our experiments: f_n and R_g are manually changed so that we reproduce the behavior observed in weak magnetic fields at temperatures around T_{cg}, H_{0J} and α_{0J} are adjusted so that we reproduce the ac magnetic field dependence of the step in χ' and the peak in χ'' at transition C, and B_{0g} and α_{0g} are adjusted so that we reproduce the ac magnetic field dependence of transition B.

The calculated results based on the Müller–Yang model are shown in Figs. 10(c) and 10(d). In our calculations, R_g was estimated to be 2 μm, and f_s was estimated to be 60%. These parameters are similar to those used in Müller's[20] work. However, our calculation contains several inconsistencies with the experiments. First, the behavior of transition C is different from that of the Josephson weak-link network, as shown in Figs. 10(a)–10(d). In our calculations, T_C^* is shifted toward lower temperatures, but $\Delta\chi_C'$ is not severely suppressed with increasing the amplitude of H_{ac}, which is a typical weak-link behavior. In contrast, in our experiments, *both* T_C^* and $\Delta\chi_C'$ are easily suppressed with increasing the strength of H_{ac}. Moreover, as shown in Figs. 5 and 6, the temperature dependences of H_B^* and H_C^* are qualitatively similar and are different from that of $H_{c2}(T)$ of bulk Sr_2RuO_4. This behavior is not consistent with a model of granular superconductivity, in which T_c of grains and T_c of the intergrain region should exhibit totally different field dependences. These results suggest that the Josephson-network scenario does not seem to be suitable for the superconductivity in the $Sr_3Ru_2O_7$ region of the eutectic crystals.

B. Scenario II

The second scenario assumes that no superconducting network is formed, but superconductors of thin-film shapes with multiple T_c are contained in the $Sr_3Ru_2O_7$ region. We consider that stacked monolayers of RuO_2 planes, which are the building block of superconducting Sr_2RuO_4, are contained in the $Sr_3Ru_2O_7$ region as stacking faults and exhibit superconductivity with different T_c depending on the number of monolayers contained in a stacking unit. Although fabrications of superconducting thin films of Sr_2RuO_4 have not been reported so far, it was reported that the T_c of thin $YBa_2Cu_3O_{7-x}$ films depends on their thickness.[25] It is also known that the $H_{c2}(T)$ curve of quasi-two-dimensional superconductors for the $H_{dc}\perp$ layer,[26] which can be regarded as a stacking of thin films, has a positive curvature near $H_{dc}=0$. The thickness of monolayers should be comparable to or less than the coherence length of Sr_2RuO_4 along the c axis ($\sim$3.3 nm) because transitions B and C would behave as bulk superconductivity if the thickness were much larger than the coherence length. This scenario is consistent with the fact that we cannot find Sr_2RuO_4 in the $Sr_3Ru_2O_7$ region by EDX analysis and PLOM images because Sr_2RuO_4 slabs with a thickness of several nanometers are too thin to find for our instruments.

Although this scenario appears to be different from the situation of scenario I, we can still calculate $\chi_{ac}(T)$ by using the Müller–Yang model after a slight modification. The modified model, which we call as a multiple superconductor

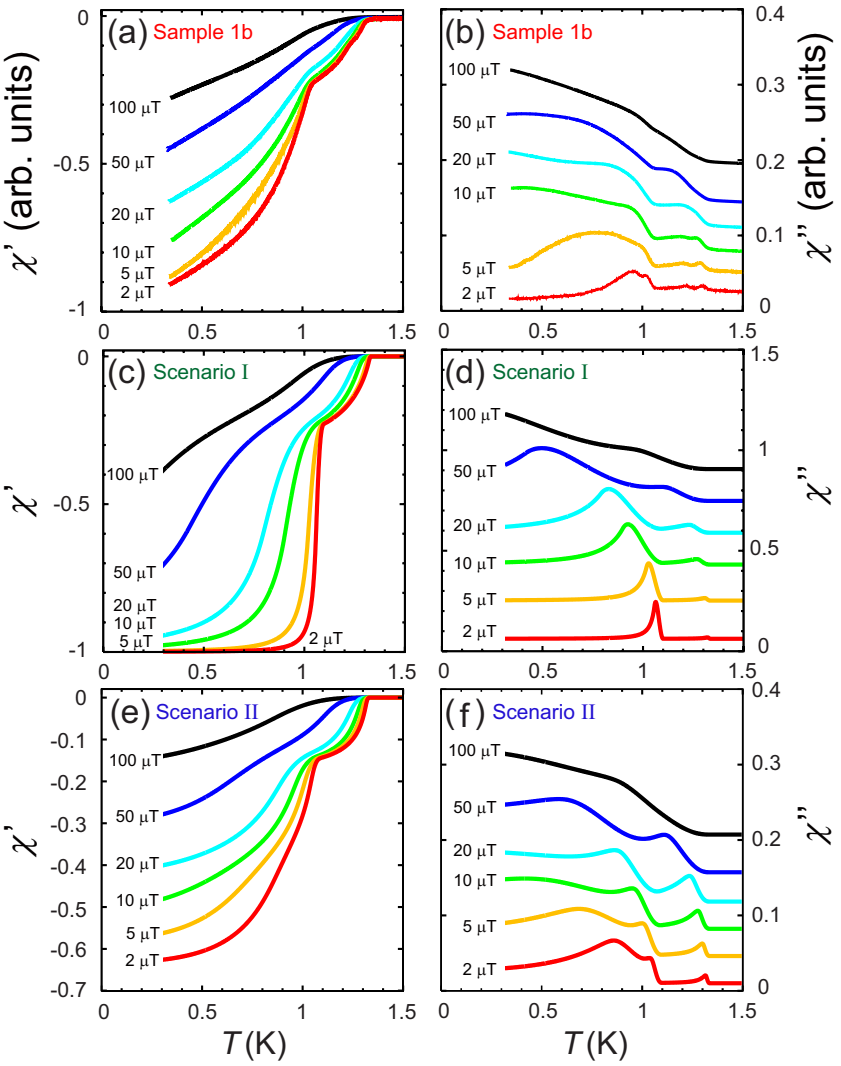

FIG. 10. (Color online) [(a) and (b)] Experimental and [(c)–(f)] calculated results of $\chi_{ac}(T)$ at various ac magnetic fields in $\mu_0 H_{dc}=0$ T. The numbers labeling the curves indicate the applied ac field amplitude $\mu_0 H_{ac}$ in μT rms.

model, assumes that the sample is divided into areas with different T_c and $\chi_{ac}(T)$ is calculated in each area by using Eqs. (1)–(6) with $\alpha_J(0)=0$ T A m^{-2} and $f_n=0$. These conditions assume that no superconducting network is formed in the sample. In this model calculation, we considered the ac susceptibility of the sample as $\chi_{ac}=\Sigma_i p_i \chi_i$, where p_i is the percentage of the ith area ($\Sigma_i p_i=1$), and χ_i represents the ac susceptibility of the ith area. It might be more plausible in reality that the thickness of a single Sr_2RuO_4 thin slab is not homogeneous. This possible inhomogeneity was neglected in our calculations.

For sample 1b, we assumed three kinds of superconductors, SC1, SC2, and SC3, with two distinct transition temperatures to reproduce the experiments well. The necessity of introducing SC3 implies that there are two kinds of regions with essentially the same T_c but with much different J_c values. These different J_c values would be caused by the effects of the finite demagnetization factor of the thin film because we embedded it into the parameters B_{0g} and $\alpha_g(0)$. However, we consider that the existence of SC3 is not essential because SC3 was not necessary in the calculations for other samples.

In our calculation, the parameters T_{cg}, $\lambda_g(0)$, and p_i were fixed. The other parameters B_{0g}, α_g, and R_g were manually adjusted so that the calculated results best agree with our experiments. The results are summarized in Table I and Figs. 10(e) and 10(f). Our calculation reproduces the essential features of the experimental findings. For example, the observation that *both* T_C^* and $\Delta\chi_C'$ decrease with increasing the amplitude of H_{ac} is reproduced. Although the critical current density $J_c(0)$ of the pure Sr_2RuO_4 is approximately 500 A/cm^2,[27] that of SC1 was estimated to be 3

TABLE I. Parameters used in our calculations based on scenario II. The open squares (□) mark the parameters that we adjusted to obtain the best fit to our experiments. The closed squares (■) label the parameters we fixed in our calculations. "SC1" denotes the superconducting area responsible for transition B and "SC2" and "SC3" denote those to transition C.

		SC1	SC2	SC3	
T_{cg}	(K)	1.34	1.10	1.10	■
B_{0g}	(μT)	10	30	200	□
$\alpha_g(0)$	(T A m^{-2})	30000	8000	3000	□
R_g	(μm)	1	1	1	□
$\lambda_g(0)$	(μm)	0.18	0.18	0.18	■
p_i		0.25	0.35	0.4	■

$\times 10^5$ A/cm^2 from B_{0g} and $\alpha_g(0)$ by using Eq. (5). If the thickness of the superconductor decreases, the cross section of the superconductor also decreases and the critical current density should become large, as are often observed in thin films. Therefore, such a large $J_c(0)$ may also support the scenario that Sr_2RuO_4 is contained as a thin slab.

No single plane of a monolayer RuO_2 probably covers the whole *ab* plane. However, the magnetic flux would be excluded from the whole sample for $H \| c$ if there are many such layers in the sample. In addition, this scenario does not contradict with our results that the apparent shielding fraction is less than 1% for $H \| ab$.

From the discussions above, we consider that this scenario is the most probable one to explain the superconductivity observed in the $Sr_3Ru_2O_7$ region of eutectic crystals. In addition, recently, such stacked monolayers of RuO_2 planes has indeed been observed by using a transmission electron microscope.[28]

C. Possibility of superconducting $Sr_3Ru_2O_7$

Finally, we discuss the possibility that small $Sr_3Ru_2O_7$ parts in sample 1b become superconducting due to a specific arrangement of the RuO_6 octahedra, which is different from the arrangement realized in bulk $Sr_3Ru_2O_7$. The structure of bulk $Sr_3Ru_2O_7$ contains orthorhombic deformations due to the rotation of the RuO_6 octahedra.[29–31] In Ruddlesden–Popper-type ruthenates $Sr_{n+1}Ru_nO_{3n+1}$, it is known that the rotation, tilting, and flattening of RuO_6 octahedra significantly affect the electronic states.[32–34] In fact, the electronic and thermodynamic properties of $Ca_{2-x}Sr_xRuO_4$ are greatly affected by the rotation with varying x.[34,35] Degrees of freedom such as the rotation angle or an ordering pattern of rotations might be left in $Sr_3Ru_2O_7$ under certain circumstances. Indeed, different ordering patterns of rotations have been reported in powder samples.[29–31] Therefore, it is possible that some small parts of $Sr_3Ru_2O_7$ with a certain arrangement of RuO_6 octahedra are superconducting and that these parts play roles of superconductors in scenario II. However, we did not obtain any direct structural evidence to conclude that octahedral rotation and/or tilting in eutectic $Sr_3Ru_2O_7$ is different from that in bulk $Sr_3Ru_2O_7$. Based on the available information, therefore, so far, we cannot conclude that $Sr_3Ru_2O_7$ itself is superconducting.

V. SUMMARY

We have studied superconductivity in the $Sr_3Ru_2O_7$-Sr_2RuO_4 eutectic system. Our ac susceptibility measurements revealed that multiple superconducting transitions occur in the $Sr_3Ru_2O_7$-Sr_2RuO_4 eutectic sample, and that the transitions with T_c lower than that of Sr_2RuO_4 originate from the $Sr_3Ru_2O_7$ region alone. These experimental results indicate that the superconductivity observed in the $Sr_3Ru_2O_7$ region is not attributable to an unusually long-range proximity effect across the boundary between Sr_2RuO_4 and $Sr_3Ru_2O_7$. Both the T^* and $\Delta\chi'$ of this superconductivity are sensibly suppressed by weak ac magnetic fields. Moreover, their *H-T* phase diagrams are qualitatively different from those of bulk Sr_2RuO_4, and no anomaly was observed in the specific heat of the $Sr_3Ru_2O_7$ region sample cut from the eutectic crystals. Although we have not achieved a conclusive explanation for the origin of superconductivity in the $Sr_3Ru_2O_7$ region, we proposed scenarios to explain our experiments. Among them, the scenario in which Sr_2RuO_4 thin slabs are embedded in the $Sr_3Ru_2O_7$ region and the multiple superconducting transition temperatures arise from the distribution of the slab thickness yielded the most satisfying fit to the experiments.

ACKNOWLEDGMENTS

We thank Franceso Tafuri, Regina Ciancio, Eva Olsson, Manfred Sigrist, Mario Cuoco, Canio Noce, Yukio Tanaka, Yasuhiro Asano, Robin S. Perry, and Andrew P. Mackenzie for valuable discussions, and Kentaro Kitagawa, Hiroshi Takatsu, and Markus Kriener for their support. This work has been supported by Grants-in-Aid for Scientific Research from the Japan Society for Promotion of Science (JSPS) and from the Ministry of Education, Culture, Sports, Science and Technology of Japan (MEXT). It was also supported by a Grant-in-Aid for the 21st Century COE program "Center for Diversity and Universality in Physics" from MEXT.

[1] Y. Maeno, H. Hashimoto, K. Yoshida, S. Nishizaki, T. Fujita, J. G. Bednorz, and F. Lichtenberg, Nature (London) **372**, 532 (1994).
[2] A. P. Mackenzie and Y. Maeno, Rev. Mod. Phys. **75**, 657 (2003).
[3] K. Ishida, H. Mukuda, Y. Kitaoka, K. Asayama, Z. Q. Mao, Y. Mori, and Y. Maeno, Nature (London) **396**, 658 (1998).
[4] G. M. Luke, Y. Fudamoto, K. M. Kojima, M. I. Larkin, J. Merrin, B. Nachumi, Y. J. Uemura, Y. Maeno, Z. Q. Mao, Y. Mori, H. Nakamura, and M. Sigrist, Nature (London) **394**, 558 (1998).
[5] J. Xia, Y. Maeno, P. T. Beyersdorf, M. M. Fejer, and A. Kapitulnik, Phys. Rev. Lett. **97**, 167002 (2006).
[6] Y. Maeno, T. Ando, Y. Mori, E. Ohmichi, S. Ikeda, S. NishiZaki, and S. Nakatsuji, Phys. Rev. Lett. **81**, 3765 (1998).
[7] R. Fittipaldi, A. Vecchione, S. Fusanobori, K. Takizawa, H. Yaguchi, J. Hooper, R. S. Perry, and Y. Maeno, J. Cryst. Growth **282**, 152 (2005).
[8] H. Yaguchi, M. Wada, T. Akima, Y. Maeno, and T. Ishiguro, Phys. Rev. B **67**, 214519 (2003).
[9] H. Yaguchi, K. Takizawa, M. Kawamura, N. Kikugawa, Y. Maeno, T. Meno, T. Akazaki, K. Semba, and H. Takayanagi, J. Phys. Soc. Jpn. **75**, 125001 (2006).
[10] M. Kawamura, H. Yaguchi, N. Kikugawa, Y. Maeno, and H. Takayanagi, J. Phys. Soc. Jpn. **74**, 531 (2005).
[11] R. S. Perry, K. Kitagawa, S. A. Grigera, R. A. Borzi, A. P. Mackenzie, K. Ishida, and Y. Maeno, Phys. Rev. Lett. **92**, 166602 (2004).

[12] R. A. Borzi, S. A. Grigera, R. S. Perry, N. Kikugawa, K. Kitagawa, Y. Maeno, and A. P. Mackenzie, Phys. Rev. Lett. **92**, 216403 (2004).
[13] J. Hooper, M. Zhou, Z. Q. Mao, Y. Liu, R. Perry, and Y. Maeno, Phys. Rev. B **73**, 132510 (2006).
[14] K. Deguchi, Z. Mao, and Y. Maeno, J. Phys. Soc. Jpn. **73**, 1313 (2004).
[15] Z. Q. Mao, Y. Mori, and Y. Maeno, Phys. Rev. B **60**, 610 (1999).
[16] K. Deguchi, M. A. Tanatar, Z. Mao, T. Ishiguro, and Y. Maeno, J. Phys. Soc. Jpn. **71**, 2839 (2002).
[17] Y. Maeno, K. Yoshida, H. Hashimoto, S. Nishizaki, S.-I. Ikeda, M. Nohara, T. Fujita, A. P. Mackenzie, N. E. Hussey, J. G. Bendnorz, and F. Lichtenberg, J. Phys. Soc. Jpn. **66**, 1405 (1997).
[18] S.-I. Ikeda, Y. Maeno, S. Nakatsuji, M. Kosaka, and Y. Uwatoko, Phys. Rev. B **62**, R6089 (2000).
[19] M. Yang, Y. H. Kao, Y. Xin, and K. W. Wong, Phys. Rev. B **50**, 13653 (1994).
[20] K. H. Müller, Physica C **159**, 717 (1989).
[21] J. R. Clem, Physica C **153-155**, 50 (1988).
[22] K. H. Müller, J. C. Macfarlane, and R. Driver, Physica C **158**, 69 (1989).
[23] A. Raboutou, J. Rosenblatt, and P. Peyral, Phys. Rev. Lett. **45**, 1035 (1980).
[24] M. Tinkham, *Introduction to Superconductivity*, 2nd ed. (McGraw-Hill, New York, 1996).
[25] M. Varela, W. Grogger, D. Arias, Z. Sefrioui, C. León, L. Vazquez, C. Ballesteros, K. M. Krishnan, and J. Santamaria, Phys. Rev. B **66**, 174514 (2002).
[26] H. Taniguchi, Y. Nakazawa, and K. Kanoda, Phys. Rev. B **57**, 3623 (1998).
[27] K. Deguchi and Y. Maeno (unpublished).
[28] R. Fittipaldi, A. Vecchione, R. Ciancio, S. Pace, M. Cuoco, D. Stornaiuolo, D. Born, T. Tafuri, E. Olsson, S. Kittaka, H. Yaguchi, and Y. Maeno, (arXiv:0712.1847v1) (unpublished).
[29] H. Shaked, J. D. Jorgensen, S. Short, O. Chmaissem, S. I. Ikeda, and Y. Maeno, Phys. Rev. B **62**, 8725 (2000).
[30] Q. Huang, J. W. Lynn, R. W. Erwin, J. Jarupatrakorn, and R. J. Cava, Phys. Rev. B **58**, 8515 (1998).
[31] Y. Inoue, M. Hara, Y. Koyama, S. Ikeda, Y. Maeno, and T. Fujita, in *Advances in Superconductivity IX*, edited by S. Nakajima and M. Murakami (Springer-Verlag, Berlin, 1997), p. 281.
[32] R. Matzdorf, Z. Fang, X. Ismail, J. Zhang, T. Kimura, Y. Tokura, K. Terakura, and E. W. Plummer, Science **289**, 746 (2000).
[33] O. Friedt, M. Braden, G. Andre, P. Adelmann, S. Nakatsuji, and Y. Maeno, Phys. Rev. B **63**, 174432 (2001).
[34] Z. Fang and K. Terakura, Phys. Rev. B **64**, 020509(R) (2001).
[35] M. Kriener, P. Steffens, J. Baier, O. Schumann, T. Zabel, T. Lorenz, O. Friedt, R. Müller, A. Gukasov, P. G. Radaelli, P. Reutler, A. Revcolevschi, S. Nakatsuji, Y. Maeno, and M. Braden, Phys. Rev. Lett. **95**, 267403 (2005).